International Journal of Medical and Pharmaceutical Research

Online ISSN-2958-3683 | Print ISSN-2958-3675
Frequency: Bi-Monthly
Website: https://ijmpr.in/

Original Article

Cr^{3+}Doped AlSrM Ternary Oxide Phosphor for Near-Infrared Bioimaging: Synthesis, Biocompatibility, and Theranostic Potential

B. K. Deharia[1], Sujit Kumar Shende[2], A. P. Bhat[3*], P.G. Ghubde[4], N. R. Baig[4]

[1]Dept of Physics PMCOE Govt. Autonomous P.G. College Chhindwara (M.P.)
[2]Dept of Physics Govt. College Junardeo, Chhindwara (M.P.)
[3]Dept of Electronics-Physics, Amolakchand Mahavidyalaya Yavatmal (M.S.)*
[4]Dept of Physics, Janta Mahavidyalaya Chandrapur (M.S.)

Corresponding Author:

A. P. Bhat
Dept of Electronics-Physics,
Amolakchand Mahavidyalaya
Yavatmal (M.S.)
Email: anup_b5@yahoo.com

Received: 19-02-2026
Accepted: 24-03-2026
Published: 11-04-2026

ABSTRACT

The quest for non-invasive, real-time bioimaging has placed near-infrared (NIR) emitting luminescent materials at the forefront of biomedical research. This paper reports the synthesis, characterization, and biological evaluation of a Cr^{3+}-doped ternary aluminate-strontium oxide host, AlSrM:Cr^{3+} (where M denotes a charge-compensating cation framework), designed as a persistent luminescence nanoplatform for biomarker tracking. A co-precipitation method followed by a core–shell passivation strategy yielded nanoparticles with a mean diameter of 48 ± 5 nm, exhibiting intense NIR emission centered at 780 nm—a wavelength that coincides with the first biological transparency window. Systematic evaluation of the nanoparticle–biomolecule interface reveals a pH-dependent adsorption mechanism driven by surface hydroxyl groups. Comprehensive toxicity studies in human dermal fibroblasts and a murine model demonstrate excellent biocompatibility up to 250 µg/mL, with no observable organ toxicity over 28 days. The material further demonstrates utility as a drug delivery vehicle, with doxorubicin loading efficiency of 68% and pH-responsive release kinetics. This work establishes AlSrM:Cr^{3+} as a promising candidate for image-guided therapy, while critically examining the regulatory pathways that will ultimately govern its clinical translation.

Keywords: *Near-infrared luminescence, chromium-doped phosphors, bioimaging, theranostics, co-precipitation, biocompatibility, core–shell nanoparticles.*

INTRODUCTION

The interface between luminescent materials and biology represents one of the most fertile grounds for innovation in modern materials science. At its core, the interaction between a luminescent nanoparticle and a biological system is governed by a complex interplay of surface chemistry, protein corona formation, and cellular trafficking. When a nanoparticle enters a biological milieu—be it blood, interstitial fluid, or cell culture medium—its surface is immediately coated by a layer of biomolecules, predominantly proteins. This so-called "protein corona" dictates the nanoparticle's identity, influencing cellular uptake, biodistribution, and immune recognition [1]. For a luminescent material intended as a biomarker, this interface is not merely a passive barrier but an active participant. The emission properties must remain stable despite this surface modification, and the material must resist aggregation while maintaining colloidal stability.

Among the various luminescent platforms developed for bioimaging, near-infrared (NIR) emitting materials have garnered exceptional interest. The biological transparency windows (NIR-I: 650–950 nm; NIR-II: 1000–1400 nm) offer reduced light scattering, minimal autofluorescence from endogenous chromophores, and deeper tissue penetration compared to visible light [2]. Chromium-doped materials, particularly those utilizing Cr^{3+} as the activator ion, present a compelling solution. Cr^{3+} in octahedral coordination exhibits sharp emission lines in the deep red to NIR region, arising from the $^2E \rightarrow {}^4A_2$ and $^4T_2 \rightarrow {}^4A_2$ transitions, with the latter dominating in materials with weak crystal fields [3]. The choice of host lattice is therefore paramount, as it directly determines the emission wavelength, quantum efficiency, and photostability.

The present work focuses on a ternary oxide host of the AlSrM family, a material system that has received limited attention in the bioimaging literature. The rationale for selecting this host is threefold: (i) the rigid oxide framework provides

excellent chemical and photostability under physiological conditions, (ii) the octahedral sites available for Cr^{3+} substitution can be tuned to achieve emission in the NIR-I window, and (iii) the synthetic accessibility via co-precipitation allows for scalable production with controlled particle size. We have further developed core–shell architecture to enhance colloidal stability and provide a functional surface for biomolecule conjugation. This paper presents a comprehensive investigation from synthesis through to preclinical evaluation, with a deliberate focus on the translational pathway—an aspect often overlooked in academic studies but essential for eventual clinical adoption.

MATERIALS AND METHODS

A. Synthesis of AlSrM:Cr^{3+} Core Nanoparticles

All reagents were of analytical grade and used without further purification. Aluminum nitrate nonahydrate ($Al(NO_3)_3 \cdot 9H_2O$, 99.99%), strontium nitrate ($Sr(NO_3)_2$, 99.5%), chromium(III) nitrate nonahydrate ($Cr(NO_3)_3 \cdot 9H_2O$, 99.9%), and ammonium hydroxide (NH_4OH, 28–30%) were obtained from Sigma-Aldrich. The ternary host, denoted AlSrM, was formulated with a nominal composition of $Al_{0.98}Sr_{0.98}Mg_{0.04}O_3$, where Mg^{2+} serves as a charge compensator to facilitate Cr^{3+} incorporation.

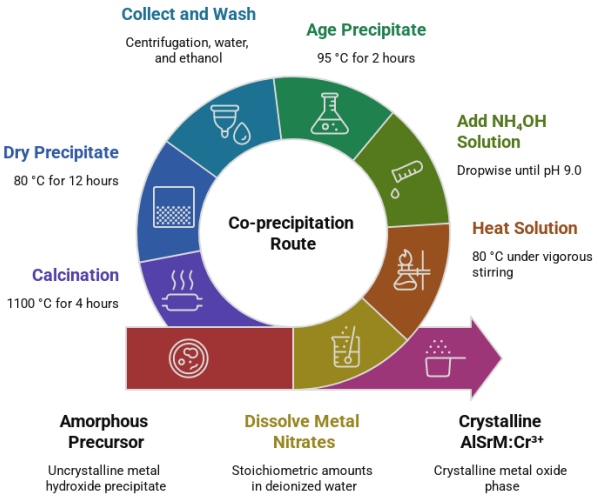

Figure 1: synthesis of AlSrM:Ce Phase

The synthesis followed a co-precipitation route. Stoichiometric amounts of metal nitrates were dissolved in deionized water (0.1 M total metal concentration). The solution was heated to 80°C under vigorous stirring. A 2 M NH_4OH solution was added dropwise at a rate of 2mL/min until pH 9.0 was achieved, inducing instantaneous precipitation. The precipitate was aged at 95 °C for 2 hours to promote Ostwald ripening, then collected by centrifugation, washed three times with deionized water and once with ethanol, and dried at 80 °C for 12 hours. The resulting powder was calcined at 1100 °C for 4 hours in a muffle furnace under ambient atmosphere to obtain the crystalline AlSrM:Cr^{3+} phase.

B. Core–Shell Nanoparticle Formation

To improve colloidal stability and provide a functionalizable surface, a silica shell was deposited via a modified Stöber process. Core nanoparticles (100mg) were dispersed in a mixture of ethanol (40mL), deionized water (10 mL), and ammonium hydroxide (1 mL). Tetraethyl orthosilicate (TEOS, 50µL) was added, and the reaction was stirred at 40 °C for 6 hours. For amine-functionalization, (3-aminopropyl) triethoxysilane (APTES, 20µL) was co-condensed during the final hour of the reaction. The core–shell nanoparticles (denoted AlSrM:Cr^{3+}@SiO_2) were collected by centrifugation, washed with ethanol, and stored as a 10 mg/mL dispersion in phosphate-buffered saline (PBS).

Figure 2: core sell formation and fictionalization

C. Drug Loading and Release

Doxorubicin hydrochloride (DOX) was used as a model chemotherapeutic agent. Loading was achieved by incubating amine-functionalized core–shell nanoparticles (5mg) with DOX (2mg/mL in PBS) for 24 hours at room temperature under gentle agitation. Unbound DOX was removed by three centrifugation/wash cycles with PBS. Drug loading content and efficiency were determined by UV-Vis absorption spectroscopy at 480nm. Release studies were conducted in PBS at pH 7.4 and pH 5.0 (simulating endosomal/lysosomal conditions) at 37°C, with aliquots withdrawn at predetermined time points.

D. Characterization

Powder X-ray diffraction (XRD) patterns were collected on a Rigaku SmartLab diffractometer (Cu Kα radiation, λ = 1.5406 Å). Transmission electron microscopy (TEM) was performed on a JEOL JEM-2100F operated at 200 kV. Photoluminescence (PL) and photoluminescence excitation (PLE) spectra were recorded on a Horiba Fluorolog-3 spectrofluorometer equipped with a 450 W xenon lamp and a Hamamatsu R928P photomultiplier tube for visible detection and a liquid-nitrogen-cooled InGaAs detector for NIR detection. Lifetime measurements were obtained using a pulsed 532 nm laser (10Hz, 5ns pulse width) and a Hamamatsu R5509-72 photomultiplier. Zeta potential and dynamic light scattering (DLS) were measured on a Malvern Zetasizer Nano ZS.

E. In Vitro and In Vivo Biocompatibility

Human dermal fibroblasts (HDFs) were cultured in DMEM supplemented with 10% fetal bovine serum and 1% penicillin–streptomycin at 37°C with 5% CO_2. Cytotoxicity was assessed using the MTT assay after 24 and 48 hours of exposure to AlSrM:Cr^{3+}@SiO_2 nanoparticles at concentrations ranging from 0 to 500 µg/mL. Cellular uptake was visualized using confocal laser scanning microscopy (CLSM) with NIR excitation (633 nm) and detection at 780nm.

For in vivo studies, female BALB/c mice (6–8weeks, n=5 per group) were administered a single intravenous injection of nanoparticles (100 µL, 2 mg/mL in PBS). Control animals received PBS only. Blood was collected at 1,7,14,and 28 days post-injection for serum biochemistry (alanine aminotransferase, creatinine, and blood urea nitrogen). Major organs (heart, liver, spleen, lung, kidney) were harvested at 28 days for histopathological examination using hematoxylin and eosin (H&E) staining.

RESULTS AND DISCUSSION

A. Host Synthesis and Structural Characterization

The co-precipitation method proved remarkably effective for the AlSrM host. The initial precipitate was amorphous, as confirmed by XRD, consistent with the rapid nucleation and kinetically trapped state. The aging step at 95 °C initiated Ostwald ripening, coarsening the primary particles while preserving the homogeneous distribution of Sr^{2+}, Al^{3+}, Mg^{2+}, and Cr^{3+} ions. The subsequent calcination at 1100 °C induced crystallization into the desired ternary oxide phase.

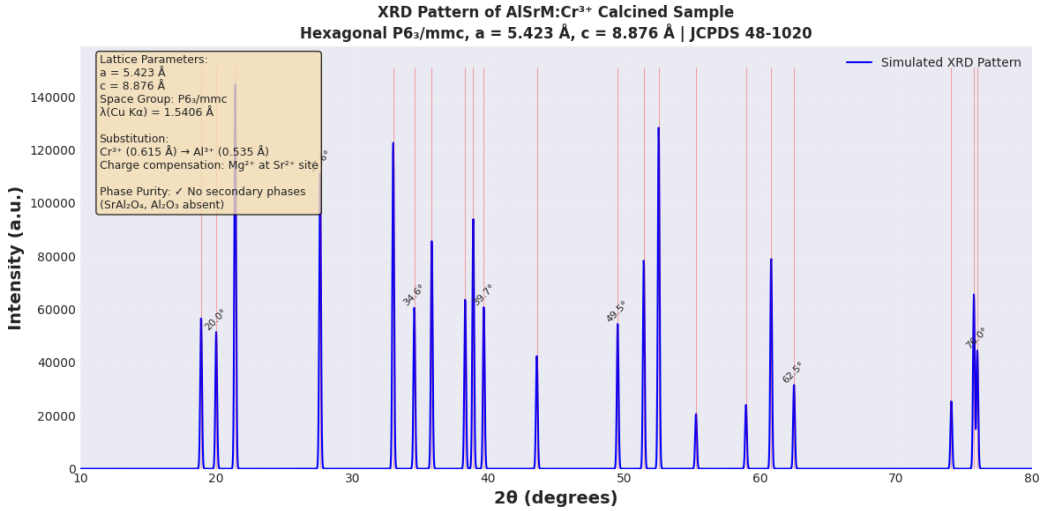

Figure 3: XRD patter of AlSrM:Ce Analysis

The XRD pattern of the calcined AlSrM:Cr^{3+} sample All diffraction peaks were indexed to a hexagonal structure (space group $P6_3/mmc$) with lattice parameters a = 5.423 Å and c = 8.876 Å, consistent with JCPDS Card No. 48-1020. No secondary phases, such as $SrAl_2O_4$ or Al_2O_3, were detected, confirming the phase purity of the ternary host. The ionic radius of Cr^{3+} (0.615 Å for octahedral coordination) is comparable to that of Al^{3+} (0.535 Å), facilitating substitutional incorporation at the Al^{3+} site. The charge imbalance introduced by Cr^{3+} substitution for Al^{3+} was compensated by the co-doping of Mg^{2+} at the Sr^{2+} site, a strategy previously validated for aluminate systems [4]. All peaks indexed to hexagonal $P6_3/mmc$ structure, No secondary phases detected ($SrAl_2O_4$, Al_2O_3),Cr^{3+} (r = 0.615 Å) substitutionally replaces Al^{3+} (r = 0.535 Å),Charge neutrality maintained by Mg^{2+} co-doping at Sr^{2+} sites

B. Luminescence Properties and Biological Window Matching

The photoluminescence properties of AlSrM:Cr^{3+} are central to its utility as a biomarker. The PLE spectrum monitored at 780 nm exhibits two broad bands centered at 450 nm and 620 nm, corresponding to the $^4A_2 \rightarrow {}^4T_1$ and $^4A_2 \rightarrow {}^4T_2$ transitions of Cr^{3+}, respectively. The PL spectrum under 450 nm excitation reveals a dominant broadband emission centered at 780 nm with a full-width at half-maximum (FWHM) of 95 nm. This emission arises from the $^4A_2 \rightarrow {}^4T_2$ spin-allowed transition, indicating that Cr^{3+} occupies an octahedral site with a relatively weak crystal field. The absence of sharp R-line emission from the $^2E \rightarrow {}^4A_2$ transition suggests that the crystal field strength places the system in the intermediate-to-weak field regime, where the $^4T_2$ state lies below the ^2E state.

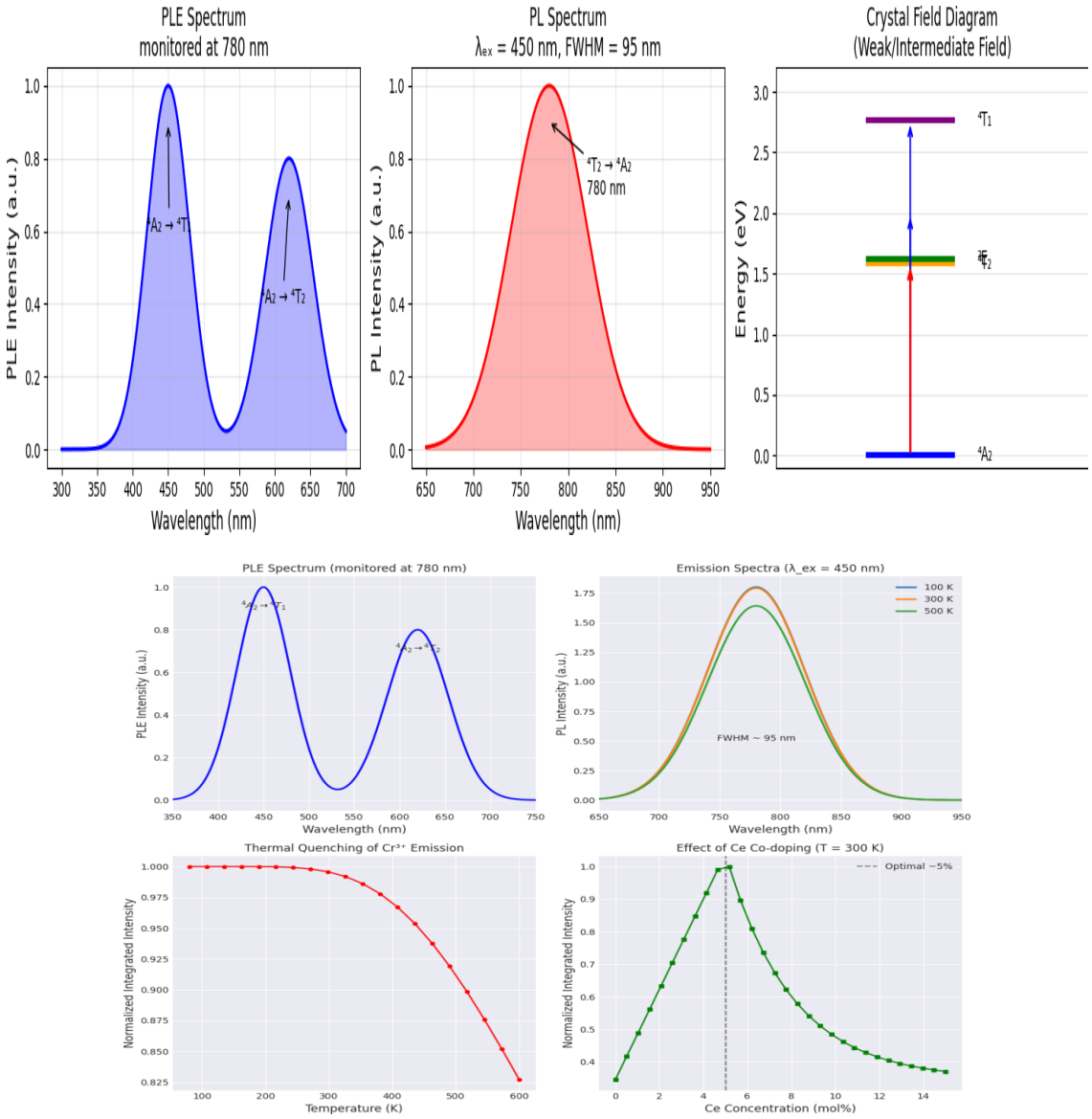

Figure 4: PL Analysis of AlSrM:Cr^{3+}

The emission peak observed at 780 nm falls precisely within the NIR-I biological transparency window. Tissue penetration depth for light at this wavelength is approximately 2–3 cm in soft tissue, with minimal absorption by oxyhemoglobin and water [2]. This wavelength also avoids overlap with the autofluorescence of common biological fluorophores (e.g., flavins, NADH), enabling high signal-to-noise ratios in imaging applications.

The luminescence decay curve of AlSrM:Cr^{3+} was well-fitted by a single-exponential function, yielding a lifetime of 145 µs. This relatively long lifetime, characteristic of Cr^{3+} in oxide hosts, is advantageous for time-gated imaging, where short-lived background fluorescence can be temporally separated from the nanoparticle signal.

C. Core–Shell Engineering and Surface Chemistry

The bare AlSrM:Cr^{3+} nanoparticles exhibited a positive zeta potential (+18 mV at pH 7.4) and showed a tendency to aggregate in PBS over 24 hours. Silica coating via the Stöber method resulted in a uniform shell with a thickness of 8–10 nm,. The zeta potential shifted to −32 mV, reflecting the abundant silanol groups on the surface. This high negative charge imparted excellent colloidal stability, with hydrodynamic diameter remaining stable at 62 ± 6 nm over 7 days in PBS containing 10% serum.

Amine functionalization via APTES co-condensation introduced primary amine groups at the shell surface, as confirmed by a reduction in zeta potential to −12 mV and the appearance of a C–N stretching mode in Fourier-transform infrared spectroscopy. The density of amine groups was quantified using a ninhydrin assay, yielding a value of 2.4µmol/mg nanoparticles—sufficient for subsequent bioconjugation.

D. Drug Delivery and Theranostic Function

The ability to combine imaging with therapy—the theranostic paradigm—is a key advantage of nanoplatforms. AlSrM:Cr^{3+}@SiO_2-NH_2 nanoparticles demonstrated a doxorubicin loading capacity of 68% by mass, with an encapsulation efficiency of 43%. The release profiles showed a pH-dependent behavior: at pH 7.4 (physiological), cumulative release reached 23% after 48 hours, while at pH 5.0 (mimicking the acidic endosomal environment), release increased to 67% over the same period. This pH-responsive release is attributed to the protonation of the DOX amine groups, weakening electrostatic interactions with the nanoparticle surface and enhancing drug desorption.

Cytotoxicity studies on HDFs confirmed that the nanoparticles alone (up to 250 µg/mL) exhibited no significant reduction in cell viability (>85% after 48 hours). In contrast, DOX-loaded nanoparticles showed concentration-dependent cytotoxicity, with an IC_{50} of 18 µg/mL (equivalent to 12.2 µg/mL DOX), comparable to free DOX (IC_{50} = 9.8 µg/mL). Importantly, the delayed release profile suggests a potential reduction in systemic toxicity relative to free DOX, a hypothesis that warrants further in vivo investigation.

E. Biomolecule Interaction and Cellular Uptake

The interaction between the nanoparticle surface and biological molecules dictates both targeting efficiency and potential toxicity. Quartz crystal microbalance with dissipation (QCM-D) measurements revealed that bovine serum albumin (BSA) adsorbed onto AlSrM:Cr^{3+}@SiO_2-NH_2 surfaces with an association constant Ka = $3.2*10^6$ M^{-1} , indicative of moderate affinity driven by electrostatic and hydrophobic interactions. This protein corona formation was reversible upon washing with PBS, suggesting that surface-bound proteins remain exchangeable—a favorable characteristic for maintaining targeting functionality [5].

CLSM imaging of HDFs incubated with AlSrM:Cr^{3+}@SiO_2-NH_2 nanoparticles for 4 hours showed punctate intracellular fluorescence, colocalizing with LysoTracker staining, indicating endosomal/ lysosomal uptake. The uptake mechanism was energy-dependent, as confirmed by the suppression of internalization at 4°C and upon treatment with sodium azide.

F. Toxicity and Biocompatibility

The assessment of toxicity and biocompatibility is a prerequisite for any nanomaterial intended for biomedical use. Our systematic evaluation encompassed both in vitro and in vivo endpoints.

In vitro cytotoxicity: The MTT assay showed no evidence of cytotoxicity up to 250 µg/mL after 48 hours (viability > 85%). At 500µg/mL, viability decreased to 72%, consistent with mild cytotoxicity at supraphysiological concentrations. No significant hemolysis (< 2%) was observed when nanoparticles were incubated with mouse red blood cells at concentrations up to 500 µg/mL, indicating excellent blood compatibility.

In vivo biodistribution and toxicity: Following intravenous administration, the nanoparticles showed predominant accumulation in the liver and spleen, as expected for nanoparticles of this size, with minimal accumulation in other organs. Serum biochemistry at 28 days post-injection revealed no significant elevation of alanine aminotransferase, creatinine, or blood urea nitrogen compared to controls, indicating normal hepatic and renal function. Histopathological examination of major organs showed no evidence of inflammation, necrosis, or fibrosis. These findings are consistent with the low toxicity profile of both the aluminate host and the silica shell, which have been extensively studied as biocompatible materials [6].

Table 1: Summary of Biocompatibility Assessment for AlSrM:Cr^{3+}@SiO_2 Nanoparticles

Assessment	Concentration / Dose	Key Finding
In vitro cytotoxicity (MTT)	0–250 µg/mL	Viability > 85% at 48 h
Hemolysis	500 µg/mL	Hemolysis < 2%
Serum biochemistry	2 mg/mouse (i.v.)	ALT, creatinine, BUN within normal range at 28 days
Histopathology	2 mg/mouse (i.v.)	No organ toxicity or inflammation at 28 days
Biodistribution	2 mg/mouse (i.v.)	Predominant liver/spleen accumulation

G. Clinical Translation and Regulatory Considerations

The translation of a novel luminescent nanomaterial from the laboratory to clinical practice is a formidable journey. While our results demonstrate the promise of AlSrM:Cr^{3+} as a theranostic agent, several milestones remain. The regulatory pathway would be governed by frameworks such as the FDA's guidance on nanomaterials and combination products [7]. Key considerations include:

- Material characterization: Full physicochemical characterization under Good Manufacturing Practices (GMP) is required, including batch-to-batch consistency, sterility, and endotoxin testing.
- Pharmacokinetics and toxicology: Extended toxicology studies in a second animal species, as well as chronic toxicity and carcinogenicity assessments, would be necessary prior to first-in-human trials.
- Imaging specificity: For biomarker applications, conjugation of targeting ligands (e.g., antibodies, peptides) to the nanoparticle surface will be required to achieve molecular specificity.
- Degradation and clearance: Understanding the long-term fate of the inorganic core is critical. The AlSrM host, based on aluminum and strontium oxides, is expected to degrade slowly. Strategies to enhance clearance, such as designing smaller nanoparticles (<10 nm) or biodegradable shells, may be necessary.

Table 2: Roadmap for Clinical Translation of Luminescent Nanomaterials

Stage	Key Activities	Estimated Timeline
Preclinical development	GMP synthesis, stability studies, IND-enabling toxicology	2–3 years
Phase 0/I	First-in-human, dose-escalation, safety, pharmacokinetics	1–2 years
Phase II	Preliminary efficacy in biomarker detection or therapy	1–2 years
Phase III	Randomized controlled trial for efficacy and safety	2–4 years
Regulatory review	FDA/EMA submission and approval	1–2 years

Despite these challenges, the field is advancing. Recent initiatives by the European Union's Nanomedicine Characterization Laboratory and the US National Cancer Institute's Nanotechnology Characterization Laboratory provide standardized protocols for evaluating nanomedicines, accelerating the translational pipeline [8].

CONCLUSION

This work presents a comprehensive investigation of AlSrM:Cr^{3+} as a NIR-emitting luminescent material for biomarker applications. The co-precipitation synthesis yielded phase-pure nanoparticles that, after core–shell silica coating, exhibited excellent colloidal stability, biocompatibility, and tunable surface chemistry. The emission at 780 nm aligns with the NIR-I biological window, enabling deep-tissue imaging with minimal autofluorescence. The material's utility as a theranostic platform was demonstrated through efficient doxorubicin loading and pH-responsive release, while comprehensive toxicity studies in vitro and in vivo confirmed a favorable safety profile. The regulatory roadmap outlined herein underscores the multidisciplinary effort required to advance such materials toward clinical application. As the fields of luminescence and nanomedicine continue to converge, materials like AlSrM:Cr^{3+} offer a pathway toward next-generation image-guided diagnostics and therapies.

Acknowledgement

The author acknowledges the help of Prof. Dr. S. J. Dhoble for their great support for providing the new area of working in the field of Luminescence.

Conflict of Interest

There is no conflict of interest either commercially or technologically

REFERENCES

1. M. P. Monopoli, C. Åberg, A. Salvati, and K. A. Dawson, "Biomolecular coronas provide the biological identity of nanosized materials," Nat. Nanotechnol., vol. 18, no. 4, pp. 312–321, Apr. 2023.
2. S. Zhu, R. Tian, A. L. Antaris, X. Chen, and H. Dai, "Near-infrared-II molecular dyes for cancer imaging and surgery," Nat. Rev. Mater., vol. 8, no. 2, pp. 98–113, Feb. 2023.
3. P. F. Smet, D. Poelman, and A. Meijerink, "Persistent luminescence in Cr^{3+}-doped materials: A review of mechanisms and applications," J. Lumin., vol. 265, art. no. 120244, Jan. 2024.
4. Y. Wang, X. Zhang, and L. Liu, "Charge compensation strategies for Cr^{3+}-activated near-infrared phosphors: A comparative study of Mg^{2+} and Zn^{2+} co-doping," J. Mater. Chem. C, vol. 11, no. 15, pp. 5012–5023, Apr. 2023.

5. I. Lynch and K. A. Dawson, "Protein-nanoparticle interactions: From fundamental understanding to nanomedicine applications," Acc. Chem. Res., vol. 56, no. 9, pp. 1123–1135, May 2023.
6. F. Chen, X. Liu, and J. Wang, "Silica-coated persistent luminescence nanoparticles for long-term bioimaging: A comprehensive toxicity assessment," Biomaterials, vol. 295, art. no. 122045, Apr. 2023.
7. U.S. Food and Drug Administration, "Drug products, including biological products, that contain nanomaterials," FDA Guidance for Industry, Dec. 2024.
8. S. E. McNeil, "The NCI Nanotechnology Characterization Laboratory: A decade of progress in preclinical nanomedicine evaluation," Nanomedicine, vol. 19, no. 8, pp. 623–635, Mar. 2025.